

Sedimentation and Flow Through Porous Media: Simulating Dynamically Coupled Discrete and Continuum Phases

Stefan Schwarzer*

*Laboratoire de Physique Mecanique des Milieux Heterogenes, Ecole Supérieure de Physique et Chimie Industrielles,
75231 Paris, Cedex 05, France*
*Höchstleistungsrechenzentrum, Forschungszentrum Jülich,
52425 Jülich, Germany*
(June 15, 2021)

Abstract

We describe a method to address efficiently problems of two-phase flow in the regime of low particle Reynolds number and negligible Brownian motion. One of the phases is an incompressible continuous fluid and the other a discrete particulate phase which we simulate by following the motion of single particles. Interactions between the phases are taken into account using locally defined drag forces. We apply our method to the problem of flow through random media at high porosity where we find good agreement to theoretical expectations for the functional dependence of the pressure drop on the solid volume fraction. We undertake further validations on systems undergoing gravity induced sedimentation.

Typeset using REVTEX

*e-mail: stefan@pmmh.espci.fr

I. INTRODUCTION

A classical problem of chemical engineering is the understanding of particulate two-phase flows, in which a continuous fluid constitutes one component and a discrete particle phase the other. The practical importance of understanding such a particle laden flow is evidenced by its central role in geophysical phenomena like sand storms, dune formation, or sediment transport, by the importance of biological questions like the understanding of the flow properties of blood, or cell component separation techniques as ultracentrifugation, by industrial applications as diverse as pneumatic transport in tubes, catalytic cracking, biological and chemical reactors, solid fuel rocket motors, fluidized beds, sedimentation, filtration and many more [1,2].

If the discreteness of the particulate phase is fully taken into account then the mathematical formulation of the flow problem involves (i) a field equation for the continuous liquid phase — in most cases the Navier-Stokes equation, subject to a set of boundary conditions both on the container walls and the surfaces of the suspended particles — and (ii) a set of differential equations for the time evolution of the degrees of freedom of the individual constituents of the particulate phase. Due to the extremely complicated boundary conditions and the nonlinearity of the underlying equations, an analytical solution to this problem is impossible, except for exceptionally simple cases. A numerical treatment, however, even with simplifying assumptions, still poses tremendous practical problems.

Several simulation techniques have been developed which we briefly review here. (a) Finite volume techniques that implement no-slip boundary conditions on the surface of each particle have been employed for very few particles. The treated Reynolds numbers [3] are in principle only limited by the grid resolution and the computation time available. Similarly, (b) lattice Boltzmann techniques for the liquid equation have been used to simulate up to 1024 suspended particles [4]. So far, these have come closest to provide realistic simulations of two-phase flows with many particles. Most other approaches involve certain assumptions that are only true in limited parameter ranges: One important class of algorithms uses the Stokesian dynamics technique [5,6] valid for low Reynolds number flow to (c) obtain the flow field consistent with no-slip boundary conditions [7] or to (d) approximate the particles as being point like [8,9].

(e) More popular in the engineering sciences, but less rigorous are continuum approximations that involve two sets of continuum equations, one for the liquid phase and one for the particulate phase. The boundary conditions on the particle surface and their influence on the flow is then represented by local drag forces depending on the solid volume fraction and local velocity differences [10,11]. In these approaches there are remaining open questions in the determination of the proper constitutive equation for the solid and the momentum exchange between the phases.

(f) To circumvent some of these later problems of the pure continuum approaches, algorithms have come into fashion that combine a discrete element [12] or molecular dynamics description [13] of the particles with a continuum equation for the liquid as in (a), but use a drag term to couple the two phases as in the pure continuum formulations (e) [14,15].

In this paper we will describe an algorithm of type (f). Such a method allows immediate access to basically all physically relevant quantities in the system, including particle coordinates and both particle and liquid velocities, at computational costs comparable to a

“standard” real space Navier-Stokes integration. The main drawback is that a neglect of the proper boundary conditions in the treatment of the liquid will result in an inaccurate rendering of the short scale flow properties. Since, however, our main focus will be the ability of the algorithm to describe collective phenomena, i.e., the effects that arise when the number of particles is large, we do not have the ambition to describe accurately the local flow fields on the scale of the particle size. At the moment the detailed effects of neglecting certain aspects of the local flow are not clear to us. Nevertheless we want to see which and how some collective phenomena emerge directly from simple modeling assumptions — as opposed to using semi-empirical expressions as, e.g., done in Refs. [14,15]. In particular, we rely on the fact that the long-range hydrodynamic interactions, which we presume to be the most important for collective phenomena, are correctly represented by the velocity and pressure fields according to the Navier-Stokes integration under consideration of an additional field representing the particle density.

The purpose of this paper is to give a detailed description of the simulation algorithm that we use to model particulate two-phase flow and its validation in the cases of (i) flow through a “porous medium” consisting of the “particles” in the simulation which are kept at fixed positions and (ii) of particles that undergo sedimentation in a suspension under the influence of gravity. In Section II we will first describe a two-dimensional implementation of the algorithm. Then, in Sec. III, we discuss first the case (i) of flow through a porous medium (Sec. III A) and second the case (ii) of sedimenting particles (Sec. III B).

II. THE ALGORITHM

We aim at a simulation of macroscopic, hard sphere particles that interact on contact when the interstitial fluid plays no important role. In addition, they interact over long-range hydrodynamic forces, mediated by an incompressible fluid medium between the particles. For the moment, we consider a two-dimensional implementation of our project. Since the analytic aspects of the solution of the Navier-Stokes equation in two dimensions are very different from the three dimensional solution, we expect at best a qualitative agreement to the features of real three dimensional flows. However, we feel justified to study the two-dimensional problem if it is possible to find qualitative knowledge on that way.

We organize the description of our algorithm into three main parts. In the first section we describe details of the employed molecular dynamics technique for the particulate phase. The second compiles the fundamental equations for the liquid phase and the details of their solution. In the third section we elaborate on the particle-liquid interaction.

A. Molecular Dynamics of the Particle Phase

1. Single particle properties and forces

Each particle i in the simulation is characterized by its radius r_i . We take the particle size distribution to be slightly polydisperse with the radii r_i drawn from a Gaussian distribution $h_p(r/\bar{r})$ with mean \bar{r} , which is cut off at its standard deviation $p\bar{r}$,

$$h_p(r/\bar{r}) \propto \begin{cases} \exp\left[-\frac{1}{2}\frac{(r/\bar{r}-1)^2}{p^2}\right], & \text{if } |r/\bar{r} - 1| < p, \\ 0, & \text{else.} \end{cases} \quad (1)$$

Here, the distribution is written in terms of the dimensionless radius r/\bar{r} and the polydispersity parameter p .

We disregard effects of rotational motion of the particles and only consider their translation. Thus we describe the particle motion only by the coordinates of their center of mass $\vec{x}_i = (x_i, y_i)$. Although the particle centers are constrained to lie in the xy plane, we will assume — for reasons that we address in Sec. II C — that the particles can otherwise be regarded as three dimensional. Therefore we associate with each particle a mass $m_i = (4/3)\pi r_i^3 \rho_p$, where ρ_p is the constant particle density.

We consider the following forces to be acting on particle i ,

$$\vec{F}_i = \frac{4}{3}\pi r_i^3(\rho_p - \rho_l)\vec{g} + \vec{F}_i^w + \vec{F}_i^d + \sum_j (\vec{F}_{ij}^n + \vec{F}_{ij}^t). \quad (2)$$

Here, \vec{F}_i is the sum of all forces on i , the \vec{F}_i^w are forces due to the presence of the boundary, the term proportional to \vec{g} accounts for particle weight and buoyancy. The drag force \vec{F}_i^d will be discussed in Sec. II C. The sum runs over the other particles in the system, but is effectively restricted to the neighborhood of particle i , since we will only introduce short range interparticle forces in radial (\vec{F}_{ij}^n) and tangential (\vec{F}_{ij}^t) direction in the next two sections.

Container walls, if present, manifest themselves by elastic forces and frictional forces in analogy to those acting between two particles. We will use for them the equations that result from those for two collision partners — to be introduced below — in the limit of the other particle having infinite mass and radius.

In direction of \vec{g} , we account for the weight of the particles. Acting opposite to gravity, we add the buoyancy reaction of the liquid, which equals the weight of the displaced fluid of constant density ρ_l . Our coordinate system is chosen such that \vec{g} points in $-y$ direction.

The forces from Eq. (2) enter the equations of motion for the particulate phase, $m_i \ddot{\vec{x}}_i = \vec{F}_i$. We solve this coupled system employing a fourth order predictor-corrector algorithm as described, e.g., in [13].

2. Pairwise interparticle forces in radial direction

At very low Reynolds numbers the lubrication forces between particles play an important role. Since they have a divergent character when the particles come close, particles in principle do not touch in this regime. However, if the fluid in the system is a gas or the particle based Reynolds numbers are not any longer small or if the particles are assumed to have some surface roughness, then they will touch and we have to model the contact forces between them.

If no fluid were present then the particles are force free unless they touch, whereupon strong repulsive and dissipative forces act between them, resulting from the viscoelastic properties of the particles. To model these forces, we here use contact models frequently employed in granular matter research [12,16,17]. The first of the forces acting on member i

of a particle pair i, j in contact is an elastic restoring force \vec{F}_{ij}^{el} . This force is proportional to the *virtual overlap* $\xi_{ij} \equiv (r_i + r_j) - |\vec{x}_i - \vec{x}_j|$ of the particles. If the overlap is positive, then

$$\vec{F}_{ij}^{\text{el}} = -k_n \xi_{ij} \vec{n}_{ij}, \quad \text{for } \xi_{ij} > 0. \quad (3)$$

Here, $\vec{n}_{ij} = (\vec{x}_j - \vec{x}_i)/|\vec{x}_j - \vec{x}_i|$ denotes the unit vector pointing from the center of particle i to the center of particle j and k_n is the stiffness of the contact, which we assume to be constant.¹ As mentioned above the force vanishes if the particles do not overlap, i.e., $\xi_{ij} < 0$.

To take the dissipative character of the contact into account, we add a velocity dependent friction term to the elastic restoring force. This damping force shall also act in the direction of the line connecting the particle centers (the *normal* direction) and be proportional to the normal relative particle velocity. On inclusion of this term, we obtain for the contact force $\vec{F}_{ij}^{c,n}$ in normal direction,

$$\vec{F}_{ij}^{c,n} = (-k_n \xi_{ij} - \gamma_n m_{\text{red}} (\dot{\vec{x}}_j - \dot{\vec{x}}_i) \cdot \vec{n}_{ij}) \vec{n}_{ij}. \quad (4)$$

In this relation, m_{red} is the reduced mass $m_i m_j / (m_i + m_j)$ of the pair in contact and γ_n determines the strength of the dissipation. We have suppressed the indices on m_{red} and γ_n , but we consider them to vary among different particle pairs.

Equation (4) is the equation for a damped harmonic oscillator while the particles are in contact. For a given initial normal relative particle velocity \vec{v}_i^n it can be solved analytically for the velocity after the contact \vec{v}_f^n . Since energy is dissipated, the ratio of these velocities is less than one; its value is termed *restitution coefficient* $e \equiv |\vec{v}_f^n|/|\vec{v}_i^n|$. One obtains for a specific particle pair (pair indices suppressed),

$$e = \exp \left[-\pi / \sqrt{\frac{4}{\gamma_n^2} \frac{k_n}{m_{\text{red}}} - 1} \right]. \quad (5)$$

However, in the presence of a liquid at low Reynolds numbers, the dominant force at small distances between pairs of particles is the lubrication force \vec{F}^l arising from the pressure necessary to replace the liquid within the gap between the two approaching spheres. The lubrication force damps the relative motion of the particles very strongly and diverges when the particles touch. Since in our approximate treatment of the liquid flow in particular the lubrication force is not well represented we add it as an additional component of the particle-particle interactions, only active at short distances between the particles. The normal component of the lubrication force is [18]

¹ The determination of k for realistic contacts in 3D is not a trivial matter. The value of k depends on the exact physical processes governing the contact and thus in general both on material constants as the Young modulus E_p or the Poisson number σ_p and the geometry of the particles. Many researchers use the nonlinear Hertzian contact theory, in which $\vec{F}_{ij}^{\text{el}} = -k_n \xi_{ij}^{3/2} \vec{n}_{ij}$. For equal sized spheres, the Hertzian theory gives $k_n = \sqrt{2r} E_p / 3(1 - \sigma_p^2)$. We refer the reader to the tables I and II for values used in the simulations.

$$\vec{F}_{ij}^{l,n} = -6\pi\eta \frac{r_{\text{red}}^2}{(-\xi_{ij})} [(\dot{\vec{x}}_i - \dot{\vec{x}}_j) \cdot \vec{n}_{ij}] \vec{n}_{ij}. \quad (6)$$

In the above equation, η denotes the shear viscosity of the liquid and r_{red} the reduced radius $r_i r_j / (r_i + r_j)$ of the pair. Again we have suppressed the indices i and j for simplicity. The expression (6) is only valid for small positive separations between the surfaces of the two involved particles. These are reflected in negative overlaps ξ_{ij} of small modulus.

To take into account the limited range of validity of Eq. (6), we cut off $\vec{F}_{ij}^{l,n}$ where $(-\xi_{ij}) > r^{\text{red}}$. To avoid a discontinuity in the force law, we subtract in Eq. (6) a constant equal to the value of the force just at this cutoff distance.

Furthermore, we remove the divergence at $\xi_{ij} = 0$ by adding to the value of $(-\xi_{ij})$ in the denominator a small positive number δr^{red} . We have used a value of $\delta = 0.1$. Other than just being a numerical contrivance our physical motivation is found in the unavoidable surface roughness of particles in reality, which may cause the particle to come into contact despite the lubrication force.

Similarly, contacts due to numerical inaccuracies are, almost unavoidable in a dense system with many particles. To cover these spurious cases as graceful as possible, we have matched the γ_n of Eq. (4) such that the force law is continuous when $\xi = 0$, for particles of radius \bar{r} . We obtain,

$$\gamma_n = 6\pi\eta \frac{r_{\text{red}}}{m_{\text{red}}} \left(\frac{1}{\delta} - \frac{1}{1+\delta} \right). \quad (7)$$

The verbal statements in the preceding three paragraphs condense into the following equations for the total interparticle forces in the normal direction, comprising both contact and lubrication forces,

$$\begin{aligned} \vec{F}_{ij}^n &= \vec{F}_{ij}^{c,n} + \vec{F}_{ij}^{l,n} \\ &= \begin{cases} \vec{0}, & \text{if } (-\xi_{ij}) > r_{\text{red}}, \\ [-6\pi\eta r_{\text{red}}^2 (\dot{\vec{x}}_j - \dot{\vec{x}}_i) \cdot \vec{n}_{ij}] \left[\frac{1}{-\xi_{ij} + \delta r_{\text{red}}} - \frac{1}{(1+\delta)r_{\text{red}}} \right] \vec{n}_{ij}, & \text{if } 0 < (-\xi_{ij}) < r_{\text{red}}, \\ [-k_n \xi_{ij} - \gamma_n m_{\text{red}} (\dot{\vec{x}}_j - \dot{\vec{x}}_i) \cdot \vec{n}_{ij}] \vec{n}_{ij}, & \text{if } \xi_{ij} > 0. \end{cases} \end{aligned} \quad (8)$$

This force is continuous over the whole range of ξ_{ij} .

3. Pairwise interparticle forces in tangential direction

To model the frictional forces acting perpendicular to the line connecting the two particle centers — the *tangential* forces — we resort, as in the case of the normal forces, to notions of particle contact modeling. Here, the Coulomb law of sliding friction asserts that the magnitude of the tangential friction force \vec{F}_{ij}^t is — on contact — proportional to the magnitude of the acting normal force \vec{F}_{ij}^n , [from Eq. (8)] with a constant of proportionality μ usually between 0.05 and 0.5,

$$|\vec{F}_{ij}^t| = \mu |\vec{F}_{ij}^n|. \quad (9)$$

This force is always directed opposite to the relative motion. Numerical problems may occur in near central impact, when the tangential component of the relative velocity is small, but

\vec{F}^n is large. Then the likewise large tangential component of the force resulting from (9) may cause an unphysical oscillatory behavior of the tangential velocity during contact. We therefore replace Eq. (9) for small relative tangential velocities by a velocity proportional friction term. Thus, finally, the tangential friction force on particle i becomes

$$\vec{F}_{ij}^t = -\min(\mu|\vec{F}_i^n|, \gamma_t|\vec{v}_{ij}^t|) \frac{\vec{v}_{ij}^t}{|\vec{v}_{ij}^t|}, \quad (10)$$

where \vec{v}_{ij}^t has been introduced as an abbreviation for the relative tangential velocity $(\dot{\vec{x}}_i - \dot{\vec{x}}_j) - [(\dot{\vec{x}}_i - \dot{\vec{x}}_j) \cdot \vec{n}_{ij}] \vec{n}_{ij}$. We do not include shear contributions of the lubrication force into the interparticle forces. For simplicity, γ_t is taken to be constant.

B. Fluid Model

We describe the state of the fluid phase by three continuum fields, namely (i) the velocity field $\vec{u}(\vec{x})$ of the fluid, (ii) its pressure $p(\vec{x})$ and (iii) a field $\epsilon(\vec{x})$ equal to the local volume fraction of liquid. These variables have only physical meaning as averages over volume on a scale larger than that of the individual particles. Their choice is motivated by continuum approaches to multiphase flow [10].

The position and geometry of the particles determines the field $\epsilon(\vec{x})$ which — for specific discrete tiling of the simulation plane — is a more or less smooth function varying between 1 (no particles) and 0 (full occupation by particles), defined for all tiles and all times. Similarly, the time evolution of the velocity field $\vec{u}(\vec{x})$ is determined by the pressure distribution, viscous contributions and a force distribution $\vec{f}(\vec{x})$ which comprises both volume forces on the liquid and momentum exchange contributions with the particulate phase (Sec. II C).

We follow Ref. [10] and write for the time evolution of the liquid velocity \vec{u} (we will drop the argument \vec{x} of the fields from now on),

$$\epsilon \rho_l \left[\frac{\partial \vec{u}}{\partial t} + (\vec{u} \nabla) \vec{u} \right] = -\epsilon \nabla p + \epsilon \eta \nabla^2 \vec{u} + \epsilon \vec{f}. \quad (11)$$

Although ϵ drops out from this equation, it enters into the the momentum exchange contribution to \vec{f} , in the sense that the momentum transfer to the particulate phase due to the fluid phase — due to drag between particles and liquid — must be “fed back” to a liquid volume smaller than in the case without particles.

Since we have in mind applications to systems with typical velocities much smaller than the velocity of sound, we can assume that the fluid phase is incompressible. The equation of liquid mass continuity then reads

$$\frac{\partial \epsilon \rho_l}{\partial t} + \nabla \cdot (\epsilon \vec{u}) = 0. \quad (12)$$

Equation (12) presents a constraint on the velocity field that must be fulfilled at all times and may be employed to obtain the pressure field via an iterative procedure which we model after the artificial compressibility method of Chorin [19–21]. Here, we sketch the basic ideas of its 2D implementation briefly and refer the reader for more details to the literature.

We discretize the differential equations (11) and (12) in the following way. We place the velocity components u_x , u_y as well as the pressure p on three quadrilateral meshes with lattice spacing Δx . With respect to the pressure grid, the grids for the x and y velocity components are shifted by $\Delta x/2$ in x and y direction respectively. This construction is commonly referred to as the MAC mesh and has several computational advantages. For instance, it is a simple means to avoid numerical instabilities due to mesh decoupling [21]. The choice of location for the computational quantities is conceptually related to location of variables in finite volume techniques for flux conservative differential equations, in which the fluxes are located on the corresponding faces of a control volume whereas the conserved quantities themselves reside in the center of the volume [22].

We obtain the pressure and the velocity components by an iterative procedure. Let the index n refer to values at time $t = t_n$ and $n+1$ to those at $t = t_{n+1} = t_n + \Delta t$ after a timestep of duration Δt . The index k shall denote an iteration index. We define $p_{n+1,0} \equiv p_n$, i.e., we start an iteration for the new pressure at time t_{n+1} with the old values at t_n . We obtain a tentative velocity field at $t = t_{n+1}$ from an evaluation of the discretized Navier-Stokes equation (11),

$$\rho_l \frac{\vec{u}_{n+1,k+1} - \vec{u}_n}{\Delta t} = -\rho_l (\vec{u}_n \nabla) \vec{u}_n - \nabla p_{n+1,k} + \vec{f}_n + \eta \nabla^2 \vec{u}_n. \quad (13)$$

where the symbol ∇ now denotes second order precise difference operators on the lattice. As mentioned above, the solid volume fraction enters implicitly through \vec{f}_n . However, since (13) is a discretized Navier-Stokes equation, its stability criteria on the MAC grid have been studied and are reported, e.g., in [21,23]. These criteria state that the values Δx and Δt are subject to the two constraints

$$\Delta t \leq \frac{4\eta}{\rho_l (|u_x^{\max}| + |u_y^{\max}|)^2}, \quad (14)$$

and

$$\Delta t \leq \frac{\rho_l (\Delta x)^2}{4\eta}. \quad (15)$$

In general, the velocity field $\vec{u}_{n+1,k+1}$ resulting from (13) considered together with ϵ_n does not satisfy the continuity equation (12). Rather, one has to conceive the continuity equation as a constraint that determines the pressure field within the fluid such that the resulting velocity field satisfies the continuity equation at all times.

To this end, one derives an iterative procedure to determine an appropriate pressure field. This procedure is based on the idea that the local violation of the continuity equation, i.e., the value of the left hand side of Eq. (12), can be used to correct the pressure field. The correction is taken in a direction such that the modulus of the violation is reduced in the next iteration step, after a new tentative velocity field has been determined. We write

$$p_{n+1,k+1} = p_{n+1,k} - \lambda \rho_l \left[\frac{\partial \epsilon_n}{\partial t} + \nabla \cdot (\epsilon_n \vec{u}_{n+1,k+1}) \right]. \quad (16)$$

Here, a large value of the parameter λ is crucial for rapid convergence. The value of λ is, however, by stability requirements constrained to

$$0 < \lambda \leq \frac{(\Delta x)^2}{4\Delta t}. \quad (17)$$

In the simulations we have chosen λ to equal its upper stability limit.

It should be noted that the values ϵ_n in Eq. (16) are not all located on the same subgrid: the time derivative is taken at the pressure points and the ϵ_n multiplying $\vec{u}_{n+1,k+1}$ is realized by different fields, each living on the same subgrid as the associated velocity component.

Once we have determined a new pressure field, we need to recalculate new velocity values consistent with the $p_{n+1,k+1}$. These velocities may be obtained using the Navier-Stokes equation (13), or equivalently, avoiding the costly reevaluation of Eq. (13), using the relation

$$\rho_l \frac{\vec{u}_{n+1,k+2} - \vec{u}_{n+1,k+1}}{\Delta t} = \nabla(p_{n+1,k+1} - p_{n+1,k}). \quad (18)$$

Iterating Eqs. (16) and (18) yields a new pressure field and after convergence a velocity field for time t_{n+1} such that the equation of continuity is satisfied.

For our purposes, the described algorithm has three advantages. It (i) generalizes straightforwardly to 3D and (ii) unlike spectral or streamfunction methods it gives immediate access to the quantities p and \vec{u} in real space. Fast access to the latter is crucial for the calculation of the particle-liquid interaction. Moreover (iii), only the chosen coarseness of the spatial and temporal discretization limits the range of Reynolds numbers addressable in the simulation. However, since the presence of the particles is communicated to the liquid among others through the field ϵ , it does not make much physical sense to use a computational grid on a scale smaller than the particle size.

For Reynolds numbers requiring such smaller grids, one could think maybe of an approach to decompose the liquid equation into an equation for the average flow and additional equations describing the fluctuations around it, in the spirit of turbulence modeling [24].

C. Interaction of Particles and Fluid

The main problem in simulations of multiphase flow that try to bypass the specification of boundary conditions on the phase boundaries is to specify an expression for the momentum exchange between fluid and particulate phase. Even for a single sphere this task is daunting [25]. For extended fixed random collections of spheres the phenomenological Ergun formula [26,27] gives the pressure gradient as a function of solid fraction and liquid velocity. Tsuji and coworkers [14,15] have used a “localized” form of the Ergun equation to estimate the force of the liquid on a sphere and obtain for pneumatic transport in pipes and fluidized beds qualitative agreement of flow patterns and quantitative agreement of some quantities.

Having the complicated situation in mind, and being aware of the significant approximation involved, we wish to explore the consequences of a very simple model for the momentum exchange. We use a local version of the “global” Stokes formula — which is just one term in the expression given by Maxey [25] for the drag on an isolated sphere under low Reynolds number conditions — to obtain the drag force acting on a sphere of radius r_i ,

$$\vec{F}_i^d = -6\pi\eta r_i[\dot{\vec{x}}_i - \vec{u}(\vec{x}_i)]. \quad (19)$$

In order to evaluate the liquid velocity field at the location of the particle we interpolate linearly the velocity values from the closest four grid points. That is to say, if the pair (x, y) denotes the coordinates of one of these four “adjacent” grid points \vec{x}_i then $w(x, y) \equiv (1 - |x_i - x|/\Delta x)(1 - |y_i - y|/\Delta x)$ is the weight associated with (x, y) ; the index i refers to the particle location. We obtain thus for some velocity component u the interpolated value $u(\vec{x}_i)$ as $u(\vec{x}_i) = \sum w(x, y)u(x, y)$. The sum extends over the four corners of the MAC grid plaquette associated with the component u into which \vec{x}_i falls.

As equation (19) resembles the 3D expression for the drag on an isolated *sphere*, we should give here a motivation for this modeling assumption. A “pure” 2D simulation should, strictly speaking, be one of rigid, parallel *cylinders*. However, at a fixed small Reynolds number, the drag per unit length of a cylinder [28] does not depend on its radius. This behavior is very different from the observations in 3D experiments, where there is a strong dependence of the drag on the size of the spheres. Thus, in particular, effects of the particle polydispersity cannot be expected to be represented properly by a model based on drag-forces of cylinders.

We therefore use Eq. (19) for the drag and refer the force (19) to a *reference length* z equal to the average particle diameter. The picture we have in mind behind this procedure is that we imagine the particle configuration repeating itself all z length units, and the liquid being infinitely extended in z direction, however both particles and liquid being constrained to motion in the xy plane. When we calculate the drag per unit volume that enters into the Navier-Stokes equation. The finite drag force (19) acts on the liquid at the location of the center of the particle and we must thus — in order to convert it to the force density required in the continuum equation — represent it by a δ -function at \vec{x}_i ,

$$\vec{F}_i^d \frac{1}{z\epsilon(\vec{x})} \delta(\vec{x} - \vec{x}_i), \quad (20)$$

in the Navier-Stokes equation. The $\epsilon(\vec{x})$ ensures that the force density is referred to the liquid fraction alone which is necessary to conserve momentum. We form the sum over all particles and add the uniform contribution of gravitation to obtain the full volume force density term,

$$\vec{f}(\vec{x}) = \vec{g} + \sum_i \vec{F}_i^d \frac{1}{z\epsilon(\vec{x})} \delta(\vec{x} - \vec{x}_i). \quad (21)$$

On our computational lattice we implement the expression (21) by distributing $\vec{F}_i^d/z(\Delta x)^2\epsilon(\vec{x})$ to the four grid points closest to \vec{x}_i . To this end, we employ the same weights as introduced for the interpolation of the velocity components above. For example, the contribution to point (x, y) is $(1 - |x_i - x|/\Delta x)(1 - |y_i - y|/\Delta x)\vec{F}_i^d/z(\Delta x)^2\epsilon(\vec{x})$.

This concludes the description of the implementation of our algorithm.

III. APPLICATION TO EXAMPLE PROBLEMS

We will now describe the results of the application of the described algorithm on selected physical problems in order to validate our approach, and assess its limitations or respectively the consequences of using the simple drag law (19).

A. Flow through porous media

As our first system, we consider the motion of a fluid through a *fixed* random assembly of particles. Our mental picture is that the particle assembly is a model for a random porous medium with very high porosity. In the simulation, we then have to keep the particles pinned to their initial positions. However, we calculate all forces acting between particles and liquid, but we only update the liquid's degrees of freedom in the computational timestep. Excluded volume effects due the presence of the particle phase and local frictional drag still influence the fluid motion. Gravity is set to zero, or equivalently the flow is considered to lie in the horizontal plane.

In x direction the system has the width L_x and boundary conditions are periodic. We impose fixed superficial flow velocities u in y -direction at the inlet and outlet of the system at $y = 0$ and $y = L_y$, where L_y denotes the height of the system. A typical arrangement of particles in a small system of $L_x/\bar{r} \approx 33$ and $L_y/L_x = 2$ at $Re_p = 3.75 \times 10^{-3}$ and the resulting stationary flow pattern is displayed in Fig. 1. The circles indicate the particles, the arrows direction and magnitude of the liquid flux obtained by multiplying the local liquid volume fraction with the flow velocity. We see how the particle volume fraction influences the flow pattern such that the current concentrates in regions with few particles present. Note that the fluid velocity is defined everywhere in space, even at points covered by particles and that the flow velocities should therefore be considered as average values over the specific grid cell. Note also that the flux vectors are not displayed at their location used for computational purposes but are extrapolated to and displayed together with the color coded pressure at the location of the pressure points.

In this system, we measure the overall pressure drop per length $\Delta p/L_y$ as a function of the overall liquid volume fraction $\bar{\epsilon}$ of the medium and the superficial liquid velocity u . In the viscous regime the pressure drop is proportional to the fluid velocity u . We evidence a constant ratio of pressure drop to fluid velocity in Fig. 2 for several orders of magnitude of the particle Reynolds number $Re_p \equiv \rho_l \bar{r} u / \eta$ at fixed “porosity” $\bar{\epsilon}$.

We report our results in terms of the friction factor

$$f_p = -\bar{r} \Delta P / \rho_l u^2 L_y, \quad (22)$$

which is, due to the linearity of the pressure drop in the viscous regime, inversely proportional to the particle Reynolds number $Re_p \equiv \rho_l \bar{r} u / \eta$. Accordingly we have plotted in Fig. 3 the product $f_p Re_p$ which — in the viscous regime — is independent of the Reynolds number. The product's value is plotted against the liquid volume fraction or porosity $\bar{\epsilon}$ based on the 3D volume of the particles divided by the box volume $L_x \times L_y \times z$, where z denotes the effective box depth introduced in Sec. II C. The three different curves in the plot indicated by symbols correspond to two different values of $z/\bar{r} = 2$ and $8/3$ and one run (lowest lying curve) where only drag between particles and fluid was considered in the simulation and the local liquid fraction $\epsilon(\vec{x})$ in Eqs. (11) and (12) was kept equal to 1. The curves for different z/\bar{r} collapse into a single universal curve. We consider this data collapse as an *a posteriori* justification of the picture of the simulated system which we have used to find a form for the momentum feedback to the liquid (Sec. II C).

Concerning the functional form of the result in 3D, the literature lists several phenomenological expressions for the porosity dependence of the friction factor [29]. Popular expressions

for $f_p Re_p$ include (i) the half-empirical Carman-Kozeny relation $f_p Re_p \sim (1 - \bar{\epsilon})^2 / \bar{\epsilon}^3$ and (ii) the phenomenological Rumpf-Gupte form $f_p Re_p \sim \bar{\epsilon}^{-5.5}$. Both relations are only valid in an intermediate range of porosity and do not apply to the limit of very high porosity or very low solid volume fraction, where one expects $f_p Re_p \sim 1 - \bar{\epsilon}$ to leading order for the following reasons. For a strongly “dilute” random medium, let us consider the solid as independent spherical “defects.” Each defect exerts the Stokes force $6\pi r\eta\tilde{u}$ on the fluid, where \tilde{u} is the interstitial fluid velocity. Thus we approximate, on the one hand, the internal rate of energy dissipation to be $6\pi r\eta\tilde{u}^2 N$, where we denote the total number of ‘defects’ in the system by N . On the other hand, externally, the pressure drop across the system and the superficial fluid velocity $u = \tilde{u}\bar{\epsilon}$ give the rate at which work is done on the system to be $\Delta PL_{xz}u$. Equating the two rates and using $(1 - \bar{\epsilon}) = (4/3)\pi r^3 N / (L_x L_y z)$ yields

$$f_p Re_p = \frac{9}{2} \frac{1 - \bar{\epsilon}}{\bar{\epsilon}^2}. \quad (23)$$

This equation correctly predicts the pressure drop to vanish in the limit of large porosity, but it is clear from the argumentation given above that its validity is restricted to the regime of large liquid volume fraction.

The solid line in Fig. 3 shows the prediction of formula (23). The simulation data compares very favorable with this prediction for the whole range of simulated effective 3D porosities $\bar{\epsilon} > 0.7$. Please note that (23) has no adjustable parameters. The agreement is surprising considering the rather crude assumptions that we have made.

In contrast, the Carman-Kozeny formula predicts the pressure drop to vanish quadratically as $\bar{\epsilon} \rightarrow 1$, and the Rumpf-Gupte formula predicts even a constant pressure drop for $\bar{\epsilon} \rightarrow 1$. However, both formulas are applicable only in the intermediate or low porosity regime so that the lack of agreement with (23) is not surprising.

B. Sedimentation

We now discuss the application of our algorithm to the more general case when both particles and liquid are mobile and important dynamical consequences arise from the coupling of the two phases. A prototype example for this case is batch settling sedimentation. Imagine a homogeneous mixture of particles and liquid being placed into a quadrilateral — or for our purposes rectangular — container and being initially at rest. If there exists a density difference between particles and liquid, then gravitational driving forces will set the particles in motion. Complicated fluid-mediated hydrodynamic interactions between the particles lead to convoluted trajectories and give rise to collective phenomena as for example anisotropic self diffusion of particles. The particles slowly settle to the bottom of the container with an average speed $\langle V(\Phi) \rangle$ that decreases as the volume fraction Φ of particles in the container increases. We have chosen here $\Phi = 1 - \bar{\epsilon}$ to follow the convention in most of the literature on sedimentation. We display a typical situation during the batch settling process in Fig. 4.

The conditions of the simulation are periodic or respectively no-slip boundary conditions in the horizontal x direction and no-slip boundary conditions in vertical y -direction. Gravity is taken to act in $-y$ direction. One denotes as the hindered settling function $f_{hs}(\Phi)$ the ratio of the sedimentation velocity $\langle V(\Phi) \rangle$ to the Stokes velocity V_S ,

$$\langle V \rangle / V_S \equiv f_{\text{hs}}(\Phi), \quad (24)$$

where

$$V_S = (2/9)(\rho_p - \rho_l)g\bar{r}^2/\eta, \quad (25)$$

which is the settling velocity of an isolated sphere in an infinitely extended fluid.

We investigate $f_{\text{hs}}(\Phi)$ for an almost monodisperse system. The particle Reynolds number $Re_p = \rho_l \bar{r} V_S / \eta$ is smaller than 1, typically $\approx 3 \times 10^{-2}$ and (ii) the “simulation box” Reynolds number $Re_b = \rho_l L_x V_S / \eta$ is 100 times larger, i. e. $Re_b \approx 3$. Furthermore, we choose the particle size large enough such that the effects of Brownian motion may be neglected, corresponding to the regime of high (iii) Peclet number. We have performed simulations and determined the settling velocity as a function of the solid fraction of the particle suspension. The following four different sets of conditions for “thought” experiments have been performed to assess the role and importance of lubrication and backflow for the simulations. In particular, simulation series

- (i) includes lubrication effects [Eq. (6)], effects of particle void fraction [Eqs. (11,12)], and periodic boundary conditions in x direction, perpendicular to gravity;
- (ii) differs from series (i) only in the respect that we have not considered the lubrication term (6). Without these lubrication forces, we choose the value of γ_n in Eq. (4) such that for pair collisions a restitution coefficient of 0.9 results [cf. Eq. (5)];
- (iii) differs from (ii) in the respect that we have additionally set the liquid fraction $\epsilon(\vec{x})$ to 1, as if the particles consisted of liquid and not of a separate solid phase. The interaction of particle and liquid phase results only from the pointlike frictional drag between the two.
- (iv) differs from (i) only in the respect that we have used no-slip boundary conditions at $x = 0$ and $x = L_x$.

Figure 5 displays the hindered settling function of case (i). The “Stokes” velocity used to normalize the data has been obtained from simulations of single spheres. In addition, we have plotted a theoretical expression (30), $f_{\text{hs}}(\Phi) = (1 - \Phi)^3$, which we will discuss later in the text (Sec. IV B). It should be noted that experiments in the viscous regime — both Re_b and Re_p much smaller than 1 — often report a correlation with a $(1 - \Phi)^n$, $n \approx 5$ dependence [30,31], the Richardson-Zaki formula [32]. It may be that in our case the larger value of \Re_b prevents us from seeing $n \approx 5$. Of course, also the nature of hydrodynamic interactions in 2D is quite different from the 3D case, such that probably only full 3D simulations see $n = 5$ [33].

The graphs in Figure 6 address the question in which way the resulting sedimentation velocities in series (ii) to (iv) differ from that in (i). To this end, we have calculated the ratios of the sedimentation velocities. First, the symbol (\diamond) denotes the ratio $\langle V^{(ii)} \rangle / \langle V^{(i)} \rangle$. Since lubrication alters the interactions between particles more significantly when the particle fraction is high, we see that the fraction deviates more and more from 1 as the solid fraction increases. The ratio becomes smaller than 1 which means that the system “without”

lubrication sediments slower. We understand this behavior taking into account the strongly damping character of the lubrication force. Such Damping forces between particles have the effect to reduce the *relative* velocity between them and thus to favor the creation of loosely connected particle agglomerates. These effects are well known for “dry” granular systems with dissipative contact interactions between particles collisions [34,35]. These particle clusters then trap some liquid within and fall as almost coherent units. Such a unit displays a larger Stokes velocity than its constituent particles since V_S is proportional to the squared radius of the falling object.

Second, we assess the effect of backflow in the simulation by setting $\epsilon(\vec{x}) = 1$ in the Navier-Stokes and the continuity equation (11,12). The particles are then effectively point-like as far as the fluid is concerned. Denoted by \square , the ratio $\langle V^{(iii)} \rangle / \langle V^{(ii)} \rangle$ starts at a value below one — which results from particularities in the momentum exchange modeling (see Sec. IV B) — and increases with volume fraction. We can estimate the effect of backflow by assuming that the average relative velocity of particles and liquid phase are the same in situations (ii) and (iii): A short calculation assuming that the average relative velocity between particles and liquid is the same in both cases predicts $\langle V^{(iii)} \rangle / \langle V^{(ii)} \rangle = 1 / (1 - \Phi) \approx 1 + \Phi$. The observed increase is less steep as expected from this relation indicating a more complicated effect as consequence of the introduction of the volume fraction field, which we do not understand at this point.

Third, we have performed a simulation with no-slip boundary conditions on the container walls instead of the periodic boundary conditions used otherwise. We denote the data points for $\langle V^{(iv)} \rangle / \langle V^{(i)} \rangle$ by the symbol \diamond . The ratio is, apart from a point at very low volume fraction, smaller than one. The liquid velocity is constrained to be zero at the container walls and hence we believe that altogether the motion of the liquid is less vehement than in the periodic case. Since particle and liquid motion are very strongly coupled — the distance that a particle has to travel in order to reach a terminal velocity is much less than a particle diameter — the on average smaller particle velocities at the container walls suffice to slow down the settling.

1. Relation of sedimentation and flow through a random medium

At this point it is interesting to note that the functional forms proposed both for the volume fraction dependence of the mean settling velocity in the sedimentation problem and for the pressure drop in the problem of flow through random media (the Rumpf-Gupte relation) are probably not independent from each other.

More precisely, it is possible to relate the formulas for the pressure drop in flow through a random medium and the settling velocity in the sedimentation problem. During the sedimentation process, one observes two shock fronts in the suspension. One front separates the densely packed particle assembly at the bottom of the vessel from the bulk of the suspension, the other the bulk from the leftover clear fluid region at the top. If the particles were frozen in their instantaneous positions by compensating the forces acting on them, then the pressure drop between these two shock fronts is just the hydrostatic pressure drop of the pure liquid. In an infinitely extended system, time averaged, each particle experiences a total force equal to the difference of its weight and buoyancy. If the particles move freely then an additional pressure difference between the two shock fronts arises because now the

liquid must support the particles. Therefore, in steady state, the arising pressure difference must just equal the difference of particle weight and buoyancy, i.e.,

$$\frac{\Delta P}{L} = \Phi(\rho_s - \rho_l)g. \quad (26)$$

Here L denotes the height difference within the two mentioned shock fronts over which the pressure drop is measured.

On the other hand, if the particles were immobile, we could apply a drag formula of the form introduced in Sec. III A for flow through random media, say $f_p Re_p = f_{rm}(\bar{\epsilon})$, to find the pressure drop $\Delta P/L$. Let in this case \tilde{u} denote the average relative velocity of liquid and particles. Then we find that

$$\begin{aligned} \frac{\Delta P}{L} &= \frac{\tilde{u}\eta}{\bar{r}^2} f_p Re_p \\ &= \frac{\tilde{u}\eta}{\bar{r}^2} f_{rm}(\bar{\epsilon}). \end{aligned} \quad (27)$$

There is no net flux of material (liquid plus particles) through an arbitrary horizontal cross section of the suspension. Thus, if the particles settle, a net upward flux of fluid with velocity $-\langle V \rangle \Phi / (1 - \Phi)$ results. The average relative velocity of particles to liquid is therefore $\tilde{u} = \langle V \rangle / (1 - \Phi)$. We now equate the expressions (26) and (27), substitute \tilde{u} , and solve for $\langle V \rangle$:

$$\langle V \rangle = \bar{r}^2(\rho_s - \rho_l) \frac{g}{\eta} \frac{\Phi(1 - \Phi)}{f_{rm}(1 - \Phi)}. \quad (28)$$

Here, we have replaced the liquid volume fraction $\bar{\epsilon}$ by the solid volume fraction $\Phi = 1 - \bar{\epsilon}$. We obtain the dimensionless hindered settling function $f_{hs}(\Phi)$ by division of this equation by V_S ,

$$f_{hs}(\Phi) \equiv \frac{\langle V \rangle}{V_S} = \frac{9}{2} \frac{\Phi(1 - \Phi)}{f_{rm}(1 - \Phi)}. \quad (29)$$

For example, if we insert the functional form of $f_{rm}(\bar{\epsilon})$ found in Eq. (23) for the regime of Stokes flow and high dilution we obtain for the hindered settling function,

$$f_{hs}(\Phi) = (1 - \Phi)^3. \quad (30)$$

For the description of experimental data one often uses the phenomenological Richardson-Zaki correlation [32],

$$f_{hs}(\Phi) = (1 - \Phi)^n, \quad (31)$$

where n takes values around 5. Theoretical arguments by Batchelor [36,37] lead to the expression

$$f_{hs}(\Phi) = 1 - 6.55\Phi \quad (32)$$

for small Φ .

For comparison with the simulation results we have plotted relation (30) in Fig. 5 as solid line.

IV. CONCLUSION AND OUTLOOK

A. General advantages of a drag-force based approach

The major advantage of a drag-force based algorithm as described here for the simulation of two-phase flows is the capability to simulate considerably large systems with relatively moderate computational requirements. At the same time one gets without efforts a physical behavior of the particulate phase circumventing the problems of continuum approaches with stress or the constitutive equation of the particulate phase. Such an algorithm is therefore a tool to obtain quick insight into collective effects of many particles. In fact, most of the known physical effects appear to be reproducible using only a very simple expression for the momentum exchange between phases.

B. Specific problems of a drag-force based approach

We list now some of the problems that we have encountered performing the present study that will be addressed in future research.

Let us first consider the behavior of a single particle in an otherwise resting liquid, both initially at rest. If the particle density is higher than the density of the liquid, the particle will experience a net force in direction of gravity. As it falls, liquid will be dragged down with it in accordance with the momentum exchange rules and the requirements of the replacement of liquid as the local liquid fraction changes. As compared to the liquid velocity far away from the particle the local velocity is closer to the particle velocity. Consequently the isolated particle experiences a drag force which does not agree with the theoretical Stokes expression into which the particle velocity and the liquid velocity at infinity enter and the resulting terminal fall velocity of the particle is larger than the theoretical Stokes velocity.²

One way to address this problem is to alter the drag law (19) by introducing a “drag-coefficient” different from 6π and dependent on the, albeit unphysical, ratio of particle size to the grid-spacing and physical parameters as the Reynolds number — this approach has been taken in [38]. However, the root of this problem lies in the treatment of the momentum exchange and indicates that a revision of its treatment is necessary.

One could imagine first that a better treatment of the momentum exchange should proceed along the lines of approximating the liquid stress tensor on the particle surface, which may be possible in the low Reynolds number regime. However, the principal limitation of our *ansatz* is that the flow velocities in the vicinity of the particle surface are not accurately rendered as required for an estimation of the stress on the particle, since we account for the flow only in an average sense.

Another possibility is to change the drag law. We have so far employed a simple Stokes expression. It is probably necessary to introduce a drag expression which additionally depends on the local particle density in addition to the local velocity difference between phases.

² This effect has been taken into account by using the measured terminal velocity of a single sphere in lieu of the theoretical Stokes velocity, for example in the scaling of the mean sedimentation velocities to obtain the hindered settling function.

We think that at least at high particle densities also particle rotation becomes important and must be included into the model. Moreover, we may have to use density dependent local viscosities in the “Navier-Stokes” equation.

In conclusion, we should and will undertake an improvement of our algorithm to tackle some of the problems listed above in the future. However, even at the present state, we have a powerful tool at hand to assess cooperative effects of many-particle systems in which hydrodynamic interactions play an important role. We have successfully modeled flow around impurities at small and moderate volume fractions and found reasonable agreement in the case of a sedimenting system.

ACKNOWLEDGMENTS

We would like to acknowledge in particular long discussions with François Feuillebois, Hans Herrmann, Wolfgang Kalthoff, and Frank Tzschorchholz. We are also grateful for discussions with D. Barnea, M. Fermigier, I. Goldhirsch, E. Guazzelli, and J. Hinch. Stefan Schwarzer thanks the scientific council of the NATO for financial support (granted through the DAAD, Bonn).

REFERENCES

- [1] J. Happel and H. Brenner, *Low Reynolds Number Hydrodynamics* (Prentice Hall, Englewood Cliffs, New Jersey, 1965).
- [2] S. L. Soo, *Fluid Dynamics of Multiphase Flow* (Blaisdell Publishing Company, Waltham (Massachusetts), Toronto, London, 1967).
- [3] J. Feng, H. H. Hu, and D. D. Joseph, *J. Fluid Mech.* **261**, 95 (1994).
- [4] A. Ladd, *J. Fluid Mech.* **271**, 311 (1994).
- [5] J. F. Brady and G. Bossis, *Ann. Rev. Fluid Mech.* **20**, 111 (1988).
- [6] B. Cichocki, B. U. Felderhof, K. Hinsen, E. Wajnryb, and J. Blawdziewicz, *J. Chem. Phys.* **100**, 3780 (1994).
- [7] A. J. C. Ladd, *J. Chem. Phys.* **88**, 5051 (1988).
- [8] F. R. da Cunha, Ph.D. thesis, University of Cambridge, Robinson College, 1995.
- [9] K. Ichiki and H. Hayakawa, *Int. J. Mod. Phys. B* **7**, 1899 (1993).
- [10] R. Jackson, in *Fluidization*, edited by D. Harrison, J. F. Davidson, and R. Clift (Academic Press, London, 1985).
- [11] G. K. Batchelor, *J. Fluid Mech.* **193**, 75 (1988).
- [12] P. Cundall and O. D. Strack, *Geotechnique* **29**, 47 (1979).
- [13] M. P. Allen and D. J. Tildesley, *Computer Simulations of Liquids* (Clarendon Press, Oxford, 1987).
- [14] Y. Tsuji, T. Tanaka, and T. Ishida, *Powder Technology* **71**, 239 (1992).
- [15] S. Yonemura, T. Tanaka, and Y. Tsuji, *ASME/FED* **166**, 303 (1993).
- [16] O. R. Walton, in *Particulate Two-Phase Flow*, edited by M. C. Roco (Butterworth-Heinemann, Boston, 1992), Chap. 25.
- [17] G. Ristow, *Annual Reviews of Computational Physics*, 275 (1995).
- [18] R. H. Davis, in *Mobile Particulate Systems*, edited by E. Guazzelli and L. Oger (Kluwer Academic Publishers, Dordrecht, 1995).
- [19] A. J. Chorin, *J. Comp. Phys.* **2**, 12 (1967).
- [20] A. J. Chorin, *J. Math. Comp.* **22**, 745 (1968).
- [21] R. Peyret and T. D. Taylor, *Computational Methods for Fluid Flow, Springer Series in Computational Physics* (Springer, New York, Berlin, Heidelberg, 1983).
- [22] S. V. Patankar, *Numerical Heat Transfer and Fluid Flow* (Hemisphere Publishing Corporation, New York, 1980).
- [23] H. Kopetsch, in *20. IFF Ferienkurs: Computersimulationen in der Physik* (KFA Jülich, Jülich, 1989).
- [24] B. E. Launder and D. B. Spalding, *Mathematical Models of Turbulence* (Academic Press, London, 1972).
- [25] M. R. Maxey and J. J. Riley, *Phys. Fluids* **26**, 883 (1983).
- [26] S. Ergun and A. A. Orning, *Ind. Eng. Chem.* **41**, 1179 (1949).
- [27] S. Ergun, *Chem. Eng. Prog.* **48**, 89 (1952).
- [28] L. D. Landau and E. M. Lifshitz, *Mécanique des Fluides*, 2nd revised and completed ed. (Mir Publishers, Moscow, 1989).
- [29] F. A. L. Dullien, *Porous Media: Fluid Transport and Pore Structure* (Academic Press, New York, London, 1979).
- [30] H. Nicolai, B. Herzhaft, E. J. Hinch, L. Oger, and E. Guazzelli, *Phys. Fluids* **7**, 12 (1995).

- [31] J.-Z. Xue, E. Herbolzheimer, M. A. Rutgers, W. B. Russel, and P. M. Chaikin, *Phys. Rev. Lett.* **69**, 1715 (1992).
- [32] J. F. Richardson and W. N. Zaki, *Trans. Instn Chem. Engrs.* **32**, 35 (1954).
- [33] A. Ladd, *J. Fluid Mech.* **271**, 285 (1994).
- [34] I. Goldhirsch and G. Zanetti, *Phys. Rev. Lett.* **70**, 1619 (1993).
- [35] S. McNamara and W. R. Young, *Phys. Fluids A* **5**, 34 (1993).
- [36] G. K. Batchelor and J. T. Green, *J. Fluid Mech.* **56**, 375 (1972).
- [37] F. Feuillebois, *J. Fluid Mech.* **139**, 145 (1984).
- [38] W. Kalthoff, S. Schwarzer, G. Ristow, and H. Herrmann (unpublished).

TABLES

L_x	system width	3	cm
L_y	system height	6	cm
z	Stokes force reference length	0.03	cm
ρ_l	liquid density	1.09	g/cm ³
η	liquid shear viscosity	0.4	g/cm s
\bar{r}	average particle radius	0.015	cm
p	polydispersity	0.1	1

TABLE I. List of parameters for the simulation of flow through porous media. Deviating parameters are stated in the text.

L_x	system width	2.5	cm
L_y	system height	5.0	cm
z	Stokes force reference length	0.05	cm
ρ_l	liquid density	1.0	g/cm ³
η	liquid shear viscosity	0.4	g/cm s
ρ_p	particle density	2.53	g/cm ³
\bar{r}	average particle radius	0.025	cm
p	polydispersity	0.01	1
k_n	repulsion constant	2.5×10^4	g/s ²
γ_t	dissipation constant	80	1/s
μ	Coulomb friction factor	0.3	1
g	gravitational acceleration	981	cm/s ²

TABLE II. List of parameters for the simulation of batch settling sedimentation. Deviating parameters are stated in the text.

FIGURES

FIG. 1. 2D Fluid flow pattern through a random assembly of “spheres.” In this figure the 2D area fraction is $\bar{\epsilon} = 0.15$ and the particle based Reynolds number $Re_p = 0.01$. Lines indicate the direction and the magnitude of the flow. Clearly visible are the effects of the mass conservation on the flow: The flow concentrates in regions with few particles and “engulfs” the particles on smaller scales.

FIG. 2. We plot the product $f_p Re_p$ of friction factor and particle Reynolds number vs. the particle Reynolds number Re_p , at constant porosity $\bar{\epsilon} = 0.93$ ($= 1 - \sum_i (4/3) \pi r_i^3 / L_x L_y z$). Apart from small statistical fluctuations due to different initial placements of the particles, the curve is constant in the regime of Reynolds numbers $\ll 1$, thus showing that the pressure drop is proportional to u as required by Darcy’s law.

FIG. 3. We plot the product $f_p Re_p$ of friction factor and particle Reynolds number vs. the volume fraction $\bar{\epsilon}$. Different curves correspond to different flow rates (Reynolds numbers) and to different values of the system “depth” $z/\bar{r} = 2$ (+), $z/\bar{r} = 8/3$ (\square). A third set of runs has been made for the case of only frictional coupling between fluid and obstacles, setting the liquid volume fraction to one everywhere (\diamond). The volume fraction $\bar{\epsilon}$ is calculated as 3D volume fraction, considering the particles as spheres and the simulation box as quadrilateral of extension $L_x \times L_y \times z$.

FIG. 4. Typical particle configurations during a batch settling simulation at $tV_S/\bar{r} = 5.2$ (a), 16 (b), 26 (c), 36 (d), 46 (e), and 56 (f) where t denotes time, V_S the Stokes velocity and \bar{r} the average particle radius. The system size is chosen to be comparatively small $L_x/\bar{r} = 80$ and $L_y/L_x = 2$; 606 particles are visible and the 2D solid area fraction $\sum_i \pi r_i^2 / L_x L_y$ is 0.10. Lines indicate the direction and amplitude of the fluid flow. Shades of gray denote the y -component of the particle velocity, dark particles move down and light ones up. It is interesting to see that there is substantial internal motion of particles in complicated vortex patterns. The particle settling is visible “on average” for example at the upper sedimentation front.

FIG. 5. Hindered settling function $f_{hs} \equiv \langle V \rangle / V_s$ for simulation series (i) (see text), including lubrication, void fraction and using periodic boundary conditions in x direction. The ordinate shows the effective 3D solid fraction Φ , which is related to the 2D area fraction of particles in a simple way, given that the radius distribution of the particles is monodisperse: $\Phi = (4/3)(\bar{r}/z)\Phi_{2D}$. The data points have been averaged over three runs with different initial conditions. The solid line is the form $f_{hs} = (1 - \Phi)^3$ proposed in the text.

FIG. 6. Ratios of sedimentation velocities vs. the effective 3D volume fraction Φ in the simulation computed under four different sets of simulation conditions (i)..(iv), for details see text. Diamonds (\diamond) denotes the ratio the computed velocity disregarding lubrication (ii) to the velocity in the “full” simulation (i). Similarly, (+) denotes the ratio of series (iii) to (ii) — no lubrication and in (iii) additionally the liquid fraction set to 1. Boxes (\square) denote the ratio (iv) to (i) for the difference between periodic and no-slip boundary conditions for the box walls. All data points have been computed using velocity averages over three runs with different initial conditions.

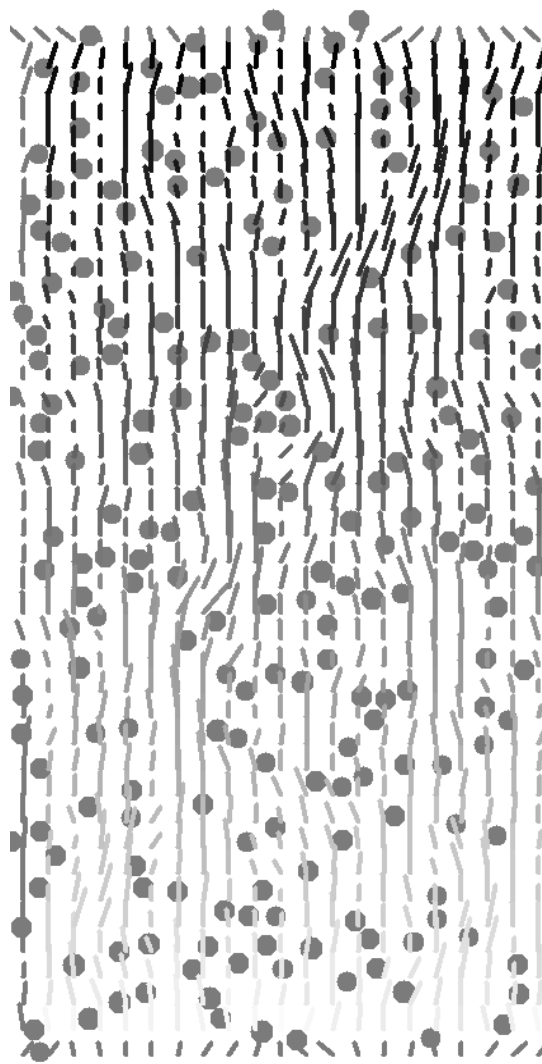


FIG. 1. 2D Fluid flow pattern through a random assembly of “spheres.” In this figure the 2D area fraction is $\bar{\epsilon} = 0.15$ and the particle based Reynolds number $Re_p = 0.01$. Lines indicate the direction and the magnitude of the flow. Clearly visible are the effects of the mass conservation on the flow: The flow concentrates in regions with few particles and “engulfs” the particles on smaller scales.

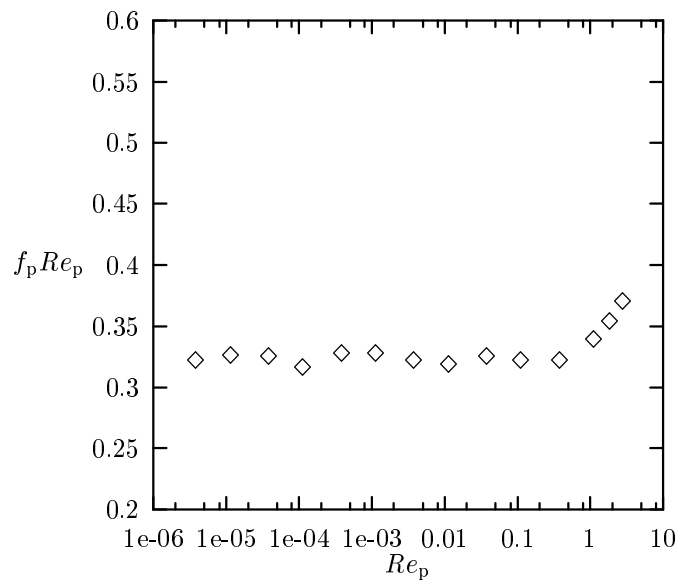


FIG. 2. We plot the product $f_p Re_p$ of friction factor and particle Reynolds number vs. the particle Reynolds number Re_p , at constant porosity $\bar{\epsilon} = 0.93$ ($= 1 - \sum_i (4/3) \pi r_i^3 / L_x L_y z$). Apart from small statistical fluctuations due to different initial placements of the particles, the curve is constant in the regime of Reynolds numbers $\ll 1$, thus showing that the pressure drop is proportional to u as required by Darcy's law.

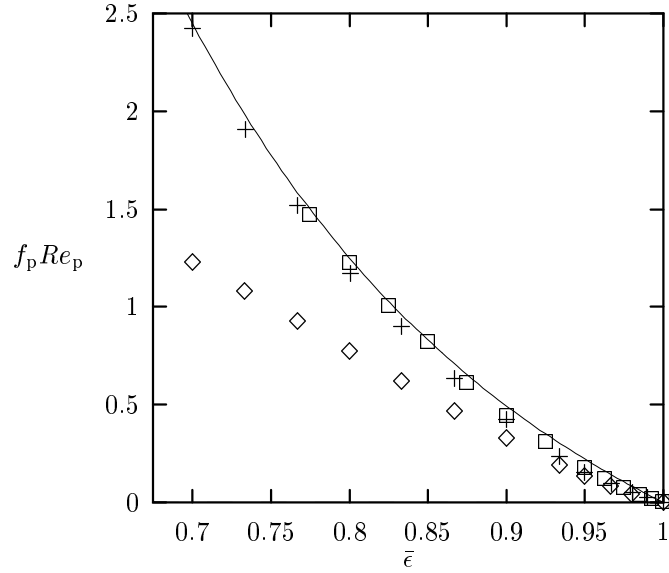


FIG. 3. We plot the product $f_p Re_p$ of friction factor and particle Reynolds number vs. the volume fraction $\bar{\epsilon}$. Different curves correspond to different flow rates (Reynolds numbers) and to different values of the system "depth" $z/\bar{r} = 2$ (+), $z/\bar{r} = 8/3$ (□). A third set of runs has been made for the case of only frictional coupling between fluid and obstacles, setting the liquid volume fraction to one everywhere (◊). The volume fraction $\bar{\epsilon}$ is calculated as 3D volume fraction, considering the particles as spheres and the simulation box as quadrilateral of extension $L_x \times L_y \times z$.

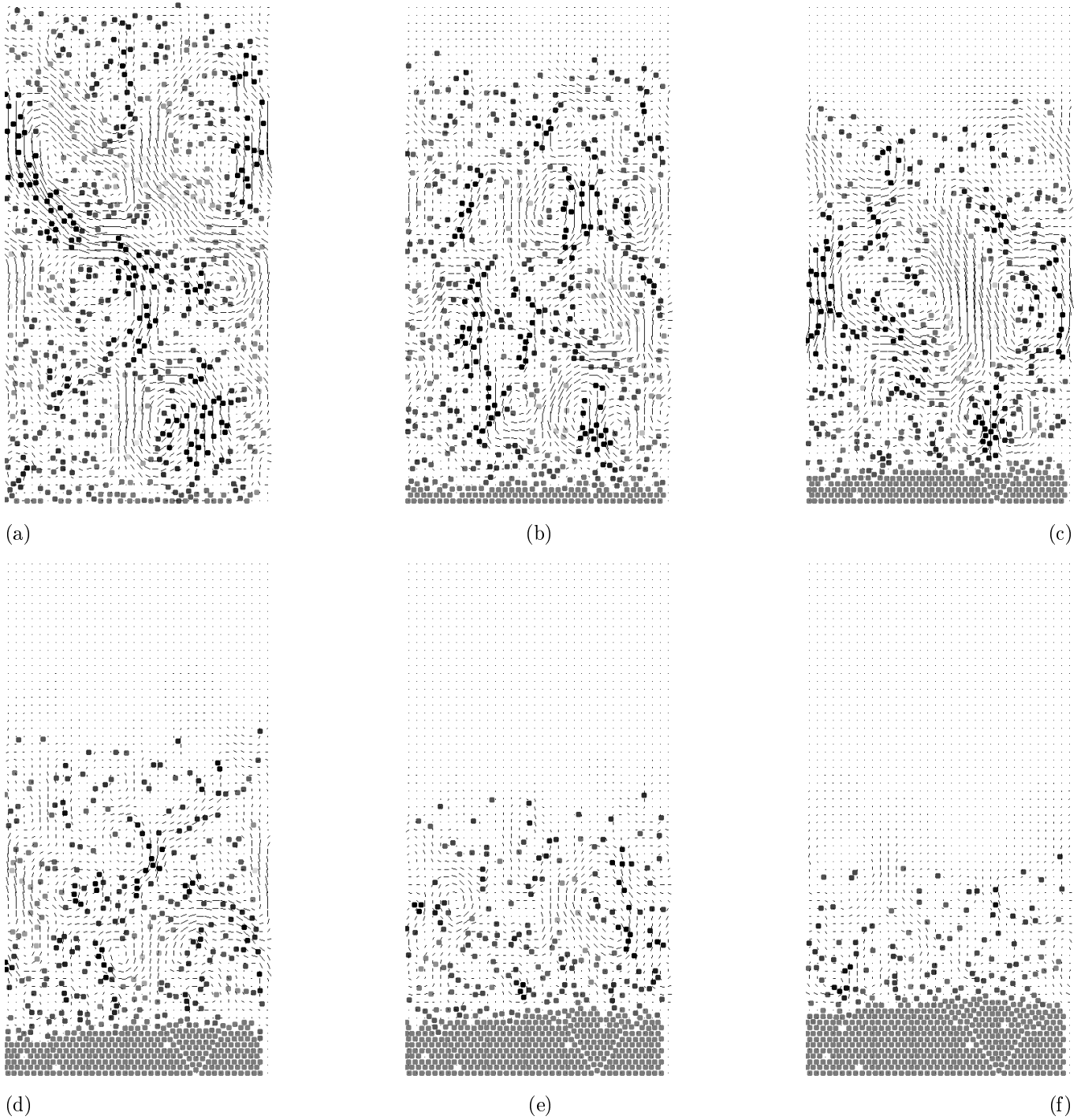


FIG. 4. Typical particle configurations during a batch settling simulation at $tV_S/\bar{r} = 5.2$ (a), 16 (b), 26 (c), 36 (d), 46 (e), and 56 (f) where t denotes time, V_S the Stokes velocity and \bar{r} the average particle radius. The system size is chosen to be comparatively small $L_x/\bar{r} = 80$ and $L_y/L_x = 2$; 606 particles are visible and the 2D solid area fraction $\sum_i \pi r_i^2/L_x L_y$ is 0.10. Lines indicate the direction and amplitude of the fluid flow. Shades of gray denote the y -component of the particle velocity, dark particles move down and light ones up. It is interesting to see that there is substantial internal motion of particles in complicated vortex patterns. The particle settling is visible “on average” for example at the upper sedimentation front.

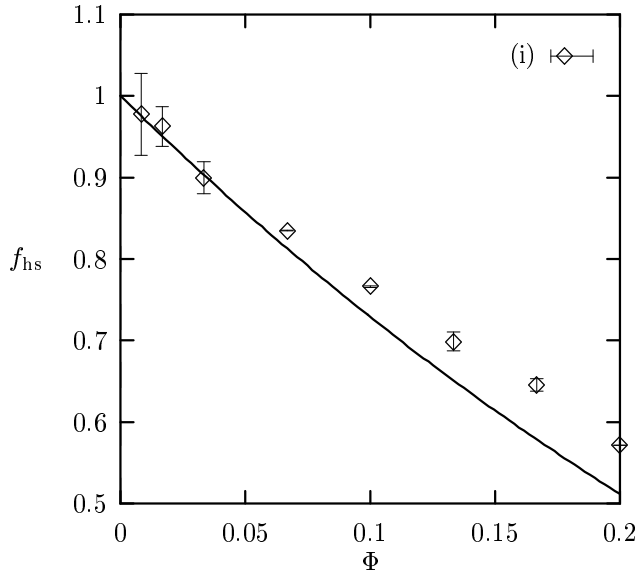


FIG. 5. Hindered settling function $f_{hs} \equiv \langle V \rangle / V_S$ for simulation series (i) (see text), including lubrication, void fraction and using periodic boundary conditions in x direction. The ordinate shows the effective 3D solid fraction Φ , which is related to the 2D area fraction of particles in a simple way, given that the radius distribution of the particles is monodisperse: $\Phi = (4/3)(\bar{r}/z)\Phi_{2D}$. The data points have been averaged over three runs with different initial conditions. The solid line is the form $f_{hs} = (1 - \Phi)^3$ proposed in the text.

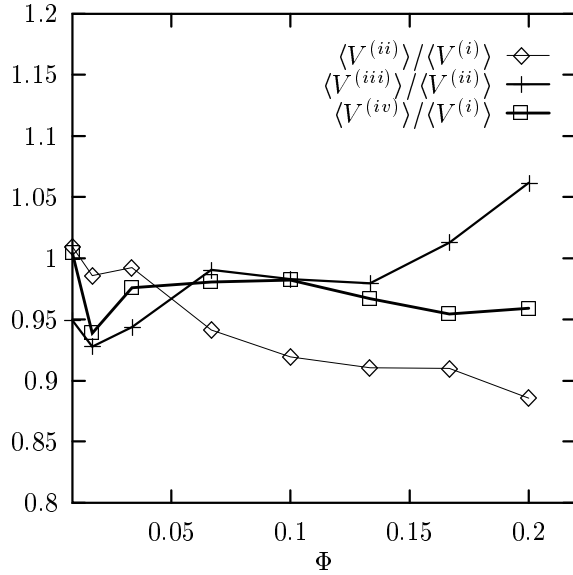


FIG. 6. Ratios of sedimentation velocities vs. the effective 3D volume fraction Φ in the simulation computed under four different sets of simulation conditions (i)..(iv), for details see text. Diamonds (◊) denotes the ratio the computed velocity disregarding lubrication (ii) to the velocity in the “full” simulation (i). Similarly, (+) denotes the ratio of series (iii) to (ii) — no lubrication and in (iii) additionally the liquid fraction set to 1. Boxes (□) denote the ratio (iv) to (i) for the difference between periodic and no-slip boundary conditions for the box walls. All data points have been computed using velocity averages over three runs with different initial conditions.